Modeling and simulation of liquid-crystal elastomers

Wei Zhu,[1,*] Michael Shelley,[2,†] and Peter Palffy-Muhoray[3,‡]

[1]*Department of Mathematics, University of Alabama, Box 870350, Tuscaloosa, Alabama 35487, USA*
[2]*Courant Institute of Mathematical Sciences, New York University, 251 Mercer Street, New York, New York 10012, USA*
[3]*Liquid Crystal Institute, Kent State University, Kent, Ohio 44242, USA*

We consider a continuum model describing the dynamic behavior of nematic liquid crystal elastomers (LCEs) and implement a numerical scheme to solve the governing equations. In the model, the Helmholtz free energy and Rayleigh dissipation are used, within a Lagrangian framework, to obtain the equations of motion. The free energy consists of both elastic and liquid crystalline contributions, each of which is a function of the material displacement and the orientational order parameter. The model gives dynamics for the material displacement, the scalar order parameter and the nematic director, the latter two of which correspond to the orientational order parameter tensor. Our simulations are carried out by solving the governing equations using an implicit-explicit scheme and the Chebyshev polynomial method. The simulations show that the model can successfully capture the shape changing dynamics of LCEs that have been observed in experiments, and also track the evolution of the order parameter tensor.

PACS number(s): 61.30.−v

I. INTRODUCTION

Liquid crystal elastomers (LCEs) are orientationally ordered solids, combining features of liquid crystals and elastic solids. They were first proposed by de Gennes [1] and first synthesized by Finkelmann *et al.* [2]. They consist of weakly cross-linked liquid crystal polymers with orientationally ordered side- or main-chain mesogenic units. They exhibit many new phenomena not found in either liquid crystals or polymers. The salient feature of LCEs is the strong coupling between mechanical deformation and orientational order. As a consequence of this coupling, mechanical strains change the order parameter and hence physical properties of LCEs, and, conversely, external stimuli, such as light, affect orientational order and can produce large shape changes [3–6].

Although many fascinating experimental results have been obtained by studying the dynamic response of LCEs to external stimuli [4,6–12], their dynamics is not fully understood. In this paper, we implement a nonlocal continuum model [13], choose and explicitly define a specific representation, and carry out numerical simulations to explore the dynamic behavior. Our work thus includes both modeling and simulation.

In the model, the Helmholtz free energy and Rayleigh dissipation are combined, using a Lagrangian approach, to obtain the dynamics. The free energy consists of both elastic and nematic contributions and includes volume conservation. As a special case of the continuum model, we choose a simple local form of the nematic free energy, the Maier-Sauper free energy, to describe nematic contributions. Our model considers only the uniaxial phase of nematic LCEs, for which the order parameter tensor can be expressed in terms of a scalar order parameter and nematic director; direct contributions to the free energy from spatial variations of the order parameter and direc-

tor are neglected. These simplifications make our model more tractable, both theoretically and numerically. Subsequently, the governing equations can be derived explicitly using both conserved and nonconserved order parameter dynamics. We thus obtain the time-dependent equations for the displacement, scalar order parameter, and nematic director.

The equations obtained are more complicated than the standard Navier-Stokes equations in the Eulerian frame. First, besides the pressure term and the viscous term, there is also an elastic term in the velocity equation. Second, our equations are written in a Lagrangian frame. This choice is straightforward for capturing the orbit as well as the dynamics within each particle in the LCE sample. Indeed, Eulerian coordinates are not well suited to our problem since the domain occupied by the LCE sample varies in time. Moreover, the derived velocity equation is very stiff due to the presence of different time scales in the problem. Simulation is therefore a fascinating but very formidable problem. In this work, we employ the Chebyshev polynomial method [14] to discretize the spatial derivatives in the dynamical equations. This method, as a typical spectral method, can achieve high accuracy and is particularly well suited to our simulation as our system is nonperiodic. We also apply the popular implicit-explicit (IMEX) schemes for the time discretization of the equations. Specifically, a combination of the second-order Adams-Bashforth method for explicit terms and the Crank-Nicolson method for implicit terms [14–16] is used.

The paper is organized as follows. In Sec. II, we give the details of the model as well as the derivation of the governing equations. To obtain the equations, we first calculate the derivatives of the free energy and dissipation densities with respect to the principal variables, that is, material displacement, order parameter, and nematic director, and then apply the appropriate conserved/nonconserved dynamics for each of the variables. In Sec. III, we present the numerics for solving the equations and then show the results of our simulations. Conclusions are given in Sec. IV.

* wzhu7@bama.ua.edu
† shelley@cims.nyu.edu
‡ mpalffy@cpip.kent.edu

II. MODELING NEMATIC LCES

To describe the dynamics of LCEs, in addition to orientational order, one needs to track the time evolution of the position of the cross-links of the LCE network. In the case of uniaxial nematic LCE, the sample can be characterized by the displacement, order parameter, and nematic direction at each Lagrangian lattice site, corresponding to a cross-link. Our work is to study how these key variables evolve in time when the sample is subjected to external stimuli. To this end, we represent the continuum model in terms of these variables, derive the governing equations, and implement the simulation by solving the equations numerically.

Our continuum model consists of the elastic free energy density and the nematic free energy density with coupling between orientational order and deformation of the network, a Rayleigh dissipation function, and a volume preserving term in the free energy. The governing equations are derived from these by applying the appropriate dynamics for each key variable. In what follows, the expressions for the free energy and the dissipation densities and their derivatives are discussed.

A. The free energy

The free energy in our model is composed of elastic and nematic contributions. The elastic free energy describes the nonlocal interaction between connected cross-links of elastomers, while the nematic free energy represents the anisotropic dispersion interactions of the mesogenic constituents.

1. The elastic free energy

Let $\boldsymbol{\alpha}$ denote an initial material position in the LCE sample and $\mathbf{x}(\boldsymbol{\alpha},t)$ be the location of that point at time t. To describe the nematic ordering in the LCE cross-linking network, an effective dimensionless step length tensor $\mathbf{L}$ is introduced, written as $\mathbf{L} = \mathbf{I} + 2\mu\mathbf{Q}$, where $\mathbf{Q}$ is the orientational order parameter tensor, $\mathbf{I}$ is the identity matrix, and μ is the dimensionless step-length anisotropy. In the uniaxial phase case, $\mathbf{Q} = S(\frac{3}{2}\mathbf{n}\mathbf{n}^T - \frac{1}{2}\mathbf{I})$, where $\mathbf{n}$ represents the unit vector along the average alignment direction of the molecular symmetry axes and S is the scalar order parameter describing the degree of alignment of the molecular axes with $\mathbf{n}$ [17].

In the undeformed state, the probability density of finding in the LCE sample a polymer chain of length $\mathcal{L}$ starting at $\boldsymbol{\alpha}$ and ending at $\boldsymbol{\alpha}'$ can be written as

$$P_0(\boldsymbol{\alpha},\boldsymbol{\alpha}') = \left(\frac{3}{2\pi\mathcal{L}b}\right)^{3/2} (\det \mathbf{L}_0)^{-1/2}$$
$$\times \exp\left(-\frac{3(\boldsymbol{\alpha}'-\boldsymbol{\alpha})^T \mathbf{L}_0^{-1}(\boldsymbol{\alpha}'-\boldsymbol{\alpha})}{2\mathcal{L}b}\right),$$

where $\mathbf{L}_0 = \mathbf{I} + 2\mu\mathbf{Q}_0$ is the effective step length at the initial state [5] and b is the persistence length. Since $\mathbf{Q}_0$ is assumed to be slowly varying compared to the distance between cross-links, we evaluate $\mathbf{Q}_0$ and $\mathbf{L}_0$ at position $(\boldsymbol{\alpha}' + \boldsymbol{\alpha})/2$. We recognize that the Gaussian distribution does not describe short chains well; we use it for simplicity, as in Ref. [5]. Although the

derivation here is for main-chain LCE, the models are expected to provide at least a qualitative description of side-chain LCEs as well.

At time t, the probability density of finding a polymer ending at $\mathbf{x}(\boldsymbol{\alpha},t)$ and $\mathbf{x}(\boldsymbol{\alpha}',t)$ shares the same form as $P_0(\boldsymbol{\alpha},\boldsymbol{\alpha}')$ with $\mathbf{L}_0(\boldsymbol{\alpha})$ being replaced by $\mathbf{L}(\boldsymbol{\alpha},t)$. The free energy of the particular polymer initially ending at $\boldsymbol{\alpha}$ and $\boldsymbol{\alpha}'$ is $-kT \ln[P(\mathbf{x}(\boldsymbol{\alpha},t),\mathbf{x}(\boldsymbol{\alpha}',t))]$, where k is the Boltzmann's constant and T is the temperature. The total elastic free energy at time t is

$$F_{\text{el}} = \frac{1}{2}\int d^3\boldsymbol{\alpha} \, \mathcal{F}_{\text{el}} = \frac{1}{2}\int d^3\boldsymbol{\alpha} \int d^3\boldsymbol{\alpha}' \, \rho_c P_0(\boldsymbol{\alpha},\boldsymbol{\alpha}')$$
$$\times(-kT \ln[P(\mathbf{x}(\boldsymbol{\alpha},t),\mathbf{x}(\boldsymbol{\alpha}',t))]) = \int d^3\boldsymbol{\alpha} \int d^3\boldsymbol{\alpha}' \, H(\boldsymbol{\alpha},\boldsymbol{\alpha}')$$
$$\times \left(\frac{3}{2\mathcal{L}b}(\mathbf{x}(\boldsymbol{\alpha}',t) - \mathbf{x}(\boldsymbol{\alpha},t))^T \mathbf{L}^{-1}(\mathbf{x}(\boldsymbol{\alpha}',t)\right.$$
$$\left. -\mathbf{x}(\boldsymbol{\alpha},t)) + \frac{1}{2}\ln \det \mathbf{L}\right), \tag{1}$$

where $\mathcal{F}_{\text{el}}$ is the elastic free energy density,

$$H(\boldsymbol{\alpha},\boldsymbol{\alpha}') = \left(\frac{1}{2}\rho_c kT\right)\left(\frac{3}{2\pi\mathcal{L}b}\right)^{3/2}(\det \mathbf{L}_0)^{-1/2}$$
$$\times \exp\left(-\frac{3(\boldsymbol{\alpha}'-\boldsymbol{\alpha})^T \mathbf{L}_0^{-1}(\boldsymbol{\alpha}'-\boldsymbol{\alpha})}{2\mathcal{L}b}\right),$$

and ρ_c is the number density of cross-links. We note that $H(\boldsymbol{\alpha},\boldsymbol{\alpha}') = H(\boldsymbol{\alpha}',\boldsymbol{\alpha})$.

2. Nematic free energy

Perhaps the most successful description of nematic order is Maier-Saupe theory. Here, the single particle potential is

$$\mathcal{E}_{\text{MS}} = -U\rho_{\text{lc}}S P_2(\cos\theta) + \frac{1}{2}U\rho_{\text{lc}}S^2,$$

where U is an interaction strength, ρ_{lc} is the number density of the liquid crystalline constituent, and S is the scalar parameter defined as $S = \langle P_2(\cos\theta)\rangle$, where θ is the angle between the symmetry axis of a mesogen and the nematic director $\mathbf{n}$. P_2 is the second Lagrange polynomial.

The nematic free energy can be written as

$$F_{\text{nem}} = \int d^3\boldsymbol{\alpha}\left[-\rho_{\text{lc}}kT \ln\left(\int \exp\left(-\frac{\mathcal{E}_{\text{MS}}}{kT}\right) d\Omega\right)\right]$$
$$= \int d^3\boldsymbol{\alpha}\left[\frac{1}{2}\rho_{\text{lc}}^2 U S^2 - \rho_{\text{lc}}kT\right.$$
$$\left. \times \ln\left(\int \exp\left(\frac{S U \rho_{\text{lc}} P_2(\cos\theta)}{kT}\right) d\Omega\right)\right], \tag{2}$$

where $d\Omega = \sin\theta d\theta d\phi$, and θ is the polar while ϕ is the azimuthal angle.

To simplify the expression for F_{nem}, we take the Taylor's series expansion of the integrand and obtain a Landau-de Gennes form for the free energy density:

$$\mathcal{F}_{\text{nem}} = \frac{1}{2}C_a S^2 - \frac{1}{3}C_b S^3 + \frac{1}{4}C_c S^4 + O(S^5), \tag{3}$$

where

$$C_a = \tfrac{1}{5}\rho_{lc}kT\left(\tfrac{\rho_{lc}U}{kT}\right)^2\left(\tfrac{5kT}{\rho_{lc}U}-1\right),$$

$$C_b = \tfrac{1}{35}\rho_{lc}kT\left(\tfrac{\rho_{lc}U}{kT}\right)^3.$$

$$C_c = \tfrac{1}{175}\rho_{lc}kT\left(\tfrac{\rho_{lc}U}{kT}\right)^4.$$

In the expressions for C_a and C_b, $5kT/\rho_{lc}U = T/T^* \approx 5/6$ and $\rho_{lc} = \tfrac{200}{3}\rho_c$, so we write C_a and C_b as

$$C_a = 500\left(\tfrac{T}{T^*}-1\right)\rho_c kT,$$
$$C_b = 400\rho_c kT,$$
$$C_c = 500\rho_c kT,$$

where $T^* \simeq 355$ K, the limit of undercooling of the isotropic phase, is very near the nematic-isotropic transition temperature.

The nematic free energy can therefore be approximated by

$$F_{nem} = \int d^3\boldsymbol{\alpha}\left(\frac{1}{2}C_a S^2 - \frac{1}{3}C_b S^3 + \frac{1}{4}C_c S^4\right).$$

3. The Rayleigh dissipation function

The total dissipated power in the system is

$$\mathcal{R} = \int d^3\boldsymbol{\alpha}\,\mathcal{R}_d, \tag{4}$$

and the Rayleigh dissipation function (dissipated power/volume) is

$$\mathcal{R}_d = \frac{1}{2}\gamma_1 \mathbf{D}:\mathbf{D} + \gamma_2 \mathbf{D}:\dot{\mathbf{Q}} + \frac{1}{2}\gamma_3\dot{\mathbf{Q}}:\dot{\mathbf{Q}},$$

where $\mathbf{D} = (\nabla_{\mathbf{x}}\mathbf{u} + \nabla_{\mathbf{x}}\mathbf{u}^T)/2$ is the symmetric rate-of-strain tensor and $\mathbf{u} = \dot{\mathbf{x}}$ and γ_i are viscosities.

To be consistent with the variable of integration $\boldsymbol{\alpha}$ in the expressions for the free energy, we rewrite the rate-of-strain $\mathbf{D}$ in terms of the Lagrangian coordinates. Indeed, note that the relation

$$\nabla_{\boldsymbol{\alpha}}\dot{\mathbf{x}} = (\nabla_{\mathbf{x}}\mathbf{u})\mathbf{F},$$

where $\mathbf{F} = \frac{\partial \mathbf{x}}{\partial \boldsymbol{\alpha}}$ is the deformation gradient, and then

$$\mathbf{D} = \frac{1}{2}[(\nabla_{\boldsymbol{\alpha}}\dot{\mathbf{x}})\mathbf{F}^{-1} + \mathbf{F}^{-T}(\nabla_{\boldsymbol{\alpha}}\dot{\mathbf{x}}^T)].$$

4. Volume preserving term in the free energy

The above free energy presents no restrictions on the sample volume. It is known, however, from experiments, that most rubbers and LCEs are nearly volume conserving [5,18]. We therefore introduce a term controlling volume:

$$F_{vol} = \frac{\Lambda}{2}\int d^3\boldsymbol{\alpha}(J-1)^2, \tag{5}$$

where $J = \det(\mathbf{F})$ and Λ is a positive constant.

B. Derivation of the governing equations

The equations of motion are determined via a Lagrangian approach, by extremizing the action in the presence of dissipation. The Lagrangian is given by

$$\mathcal{L} = \int d^3\boldsymbol{\alpha}(\mathcal{E}_{kin} - \mathcal{F}),$$

where $\mathcal{E}_{kin}$ is the kinetic energy density and $\mathcal{F}$ is the free energy density. The reactive forces are obtained from the variation of the free energy, while dissipative forces are obtained from the variation of the dissipation function. Following Ref. [13], we use the notation that if

$$F[\phi] = \int \mathcal{F}(\phi(\boldsymbol{\alpha}))d^3\boldsymbol{\alpha}, \tag{6}$$

then

$$\lim_{\epsilon\to 0}\frac{1}{\epsilon}[F[\phi+\epsilon g]-F[\phi]] = \int \frac{\delta\mathcal{F}}{\delta\phi}g\,d^3\boldsymbol{\alpha}. \tag{7}$$

Note that this differs somewhat from a more conventional notation [19], but it is dimensionally consistent and maintains consistency with our previous work [4].

The equations of motion for the system are

$$\frac{\partial}{\partial t}\frac{\delta\mathcal{E}_{kin}}{\delta\dot{\mathbf{x}}} + \frac{\delta\mathcal{F}}{\delta\mathbf{x}} + \frac{\delta\mathcal{R}_d}{\delta\dot{\mathbf{x}}} = 0, \tag{8}$$

$$\frac{\delta\mathcal{F}}{\delta S} + \frac{\delta\mathcal{R}_d}{\delta\dot{S}} = 0, \tag{9}$$

and

$$\frac{\delta\mathcal{F}}{\delta\mathbf{n}} + \frac{\delta\mathcal{R}_d}{\delta\dot{\mathbf{n}}} = 0, \tag{10}$$

where we have assumed that the kinetic energy associated with changes in the scalar order parameter S and the nematic director $\mathbf{n}$ can be neglected. To derive the equations of motion for the displacement ($\mathbf{x}$), order parameter (S), and nematic director ($\mathbf{n}$), one needs to calculate the derivatives of $\mathcal{F}_{el}$, $\mathcal{F}_{nem}$, and $\mathcal{F}_{vol}$ with respect to $\mathbf{x}$, S, and $\mathbf{n}$ and of the kinetic energy $\mathcal{E}_{kin}$ and dissipation $\mathcal{R}_d$ with respect to $\dot{\mathbf{x}}$, $\dot{S}$, and $\dot{\mathbf{n}}$.

1. Derivatives of elastic free energy

The elastic free energy is given by $F_{el} = \int d^3\boldsymbol{\alpha}\,\mathcal{F}_{el}(\boldsymbol{\alpha})$ where

$$\mathcal{F}_{el}(\boldsymbol{\alpha}) = \int d^3\boldsymbol{\alpha}' H(\boldsymbol{\alpha},\boldsymbol{\alpha}')\left(\frac{3}{2\mathcal{L}b}(\mathbf{x}(\boldsymbol{\alpha}',t)-\mathbf{x}(\boldsymbol{\alpha},t))^T\right.$$
$$\left.\times\mathbf{L}^{-1}(\mathbf{x}(\boldsymbol{\alpha}',t)-\mathbf{x}(\boldsymbol{\alpha},t)) + \frac{1}{2}\ln\det\mathbf{L}\right). \tag{11}$$

We calculate the derivative of the free energy density and illustrate the method in some detail. Let $\mathbf{y} = \mathbf{y}(\boldsymbol{\alpha})$ be an arbitrary function. For convenience, we denote $\Delta\mathbf{x}_i = \mathbf{x}_i(\boldsymbol{\alpha}',t)-\mathbf{x}_i(\boldsymbol{\alpha},t)$, $\Delta\mathbf{y}_i = \mathbf{y}_i(\boldsymbol{\alpha}')-\mathbf{y}_i(\boldsymbol{\alpha})$, and $g(\mathbf{x}) = (\mathbf{x}(\boldsymbol{\alpha}',t)-\mathbf{x}(\boldsymbol{\alpha},t))^T\mathbf{L}(\boldsymbol{\alpha},t)^{-1}(\mathbf{x}(\boldsymbol{\alpha}',t)-\mathbf{x}(\boldsymbol{\alpha},t))$. Then for $|\epsilon| \ll 1$,

$$g(\mathbf{x}+\epsilon\mathbf{y}) = \mathbf{L}_{ij}^{-1}(\boldsymbol{\alpha},t)(\Delta\mathbf{x}_i + \epsilon\Delta\mathbf{y}_i)(\Delta\mathbf{x}_j + \epsilon\Delta\mathbf{y}_j)$$
$$= g(\mathbf{x}) + \epsilon\mathbf{L}_{ij}^{-1}(\boldsymbol{\alpha},t)(\Delta\mathbf{x}_i\Delta\mathbf{y}_j + \Delta\mathbf{x}_j\Delta\mathbf{y}_i) + O(\epsilon^2).$$

One gets

$$\lim_{\epsilon \to 0} \frac{1}{\epsilon}(g(\mathbf{x} + \epsilon \mathbf{y}) - g(\mathbf{x})) = \mathbf{L}_{ij}^{-1}(\boldsymbol{\alpha},t)(\Delta \mathbf{x}_i \Delta \mathbf{y}_j + \Delta \mathbf{x}_j \Delta \mathbf{y}_i),$$

and then

$$\lim_{\epsilon \to 0} \frac{1}{\epsilon}(F_{\text{el}}[\mathbf{x} + \varepsilon \mathbf{y}] - F_{\text{el}}[\mathbf{x}])$$

$$= \int d^3\boldsymbol{\alpha} \int d^3\boldsymbol{\alpha}' H(\boldsymbol{\alpha},\boldsymbol{\alpha}') \left(\frac{3}{2\mathcal{L}b}\right)$$

$$\times \mathbf{L}_{ij}^{-1}(\boldsymbol{\alpha},t)(\Delta \mathbf{x}_i \Delta \mathbf{y}_j + \Delta \mathbf{x}_j \Delta \mathbf{y}_i)$$

$$= \int d^3\boldsymbol{\alpha} \int d^3\boldsymbol{\alpha}' H(\boldsymbol{\alpha},\boldsymbol{\alpha}') \left(\frac{3}{2\mathcal{L}b}\right)$$

$$\times \left[-2[\mathbf{L}_{ij}^{-1}(\boldsymbol{\alpha},t) + \mathbf{L}_{ij}^{-1}(\boldsymbol{\alpha}',t)]\Delta \mathbf{x}_i \mathbf{y}_j(\boldsymbol{\alpha})\right].$$

Therefore, the derivative of the elastic free energy density $\mathcal{F}_{\text{el}}$ is

$$\frac{\delta \mathcal{F}_{\text{el}}}{\delta \mathbf{x}} = -2 \int d^3\boldsymbol{\alpha}' H(\boldsymbol{\alpha},\boldsymbol{\alpha}') \left(\frac{3}{2\mathcal{L}b}\right)$$

$$\times [\mathbf{L}^{-1}(\boldsymbol{\alpha},t) + \mathbf{L}^{-1}(\boldsymbol{\alpha}',t)](\mathbf{x}(\boldsymbol{\alpha}',t) - \mathbf{x}(\boldsymbol{\alpha},t)).$$

We proceed similarly to calculate $\delta \mathcal{F}_{\text{el}}/\delta S$, and get

$$\frac{\delta \mathcal{F}_{\text{el}}}{\delta S} = \int d^3\boldsymbol{\alpha}' H(\boldsymbol{\alpha},\boldsymbol{\alpha}')\left[\frac{1}{2}\frac{-6\mu S}{(1 - \mu S)(1 + 2\mu S)} + \frac{3}{2\mathcal{L}b}\frac{1}{(1 - \mu S)^2}(\mathbf{x}(\boldsymbol{\alpha}) - \mathbf{x}(\boldsymbol{\alpha}'))^T \left(\mathbf{I} - \frac{3(2\mu^2 S^2 + 1)}{(2\mu S + 1)^2}\mathbf{n}\mathbf{n}^T\right)(\mathbf{x}(\boldsymbol{\alpha}) - \mathbf{x}(\boldsymbol{\alpha}'))\right]. \tag{12}$$

We next find $\delta \mathcal{F}_{\text{el}}/\delta \mathbf{n}$. Proceeding as above, we obtain

$$\frac{\delta \mathcal{F}_{\text{el}}}{\delta \mathbf{n}} = \int d^3\boldsymbol{\alpha}' H(\boldsymbol{\alpha},\boldsymbol{\alpha}')\frac{3}{2\mathcal{L}b}\frac{-6\mu S}{(1 - \mu S)(2\mu S + 1)}[(\mathbf{n} \cdot (\mathbf{x}(\boldsymbol{\alpha}) - \mathbf{x}(\boldsymbol{\alpha}')))(\mathbf{x}(\boldsymbol{\alpha}) - \mathbf{x}(\boldsymbol{\alpha}')) - (\mathbf{n} \cdot (\mathbf{x}(\boldsymbol{\alpha}) - \mathbf{x}(\boldsymbol{\alpha}')))^2 \mathbf{n}]. \tag{13}$$

The purpose of the nonlocal description in the model rather than a gradient expansion is to ensure that no artifacts arise in the dynamical equations due to truncation of the gradient expansion when the variation is carried out [20]. Once the derivatives have been evaluated, gradient expansions can safely be carried out. Since evaluation of the integrals is cumbersome and computationally expensive, we turn here to long-wavelength expansions of the integrands and apply these to $\delta \mathcal{F}_{\text{el}}/\delta \mathbf{x}$, $\delta \mathcal{F}_{\text{el}}/\delta S$, and $\delta \mathcal{F}_{\text{el}}/\delta \mathbf{n}$.

Let $\boldsymbol{\alpha}' - \boldsymbol{\alpha} = (\frac{3}{2\mathcal{L}b})^{-1/2}\mathbf{L}_0^{1/2}\boldsymbol{\beta}$; then

$$d^3\boldsymbol{\alpha}' = \left(\frac{3}{2\mathcal{L}b}\right)^{-3/2} \det(\mathbf{L}_0)^{1/2}d^3\boldsymbol{\beta},$$

$$H(\boldsymbol{\alpha},\boldsymbol{\alpha}') = \left(\frac{1}{2}\rho k T\right) \left(\frac{3}{2\pi \mathcal{L}b}\right)^{3/2} (\det \mathbf{L}_0)^{-1/2} \exp(-\boldsymbol{\beta} \cdot \boldsymbol{\beta}),$$

$$\mathbf{L}^{-1}(\boldsymbol{\alpha},t) + \mathbf{L}^{-1}(\boldsymbol{\alpha}',t) \simeq 2\mathbf{L}^{-1}(\boldsymbol{\alpha},t) + \frac{\partial \mathbf{L}^{-1}}{\partial \boldsymbol{\alpha}}\left(\frac{3}{2\mathcal{L}b}\right)^{-1/2}\mathbf{L}_0^{1/2}\boldsymbol{\beta},$$

and

$$\mathbf{x}(\boldsymbol{\alpha}') - \mathbf{x}(\boldsymbol{\alpha}) \simeq \frac{\partial \mathbf{x}}{\partial \boldsymbol{\alpha}}\left(\frac{3}{2\mathcal{L}b}\right)^{-1/2}\mathbf{L}_0^{1/2}\boldsymbol{\beta} + \frac{1}{2}\frac{\partial^2 \mathbf{x}}{\partial \boldsymbol{\alpha}_1 \partial \boldsymbol{\alpha}_2}\left(\frac{3}{2\mathcal{L}b}\right)^{-1/2}\mathbf{L}_0^{1/2}\boldsymbol{\beta}_1\left(\frac{3}{2\mathcal{L}b}\right)^{-1/2}\mathbf{L}_0^{1/2}\boldsymbol{\beta}_2.$$

To make the expression of $\delta \mathcal{F}_{\text{el}}/\delta \mathbf{x}$ clear, we here consider its ith component

$$\left(\frac{\delta \mathcal{F}_{\text{el}}}{\delta \mathbf{x}}\right)_i = -2\pi^{-3/2}\left(\frac{1}{2}\rho_c k T\right)\int d^3\boldsymbol{\beta} \exp(-\boldsymbol{\beta} \cdot \boldsymbol{\beta})[\mathbf{L}_{ij}^{-1}(\boldsymbol{\alpha})\frac{\partial^2 \mathbf{x}_j}{\partial \boldsymbol{\alpha}_p \partial \boldsymbol{\alpha}_q}\mathbf{L}_{0,pm}^{1/2}\boldsymbol{\beta}_m \mathbf{L}_{0,qn}^{1/2}\boldsymbol{\beta}_n + \frac{\partial \mathbf{L}_{ij}^{-1}(\boldsymbol{\alpha})}{\partial \boldsymbol{\alpha}_s}\left(\mathbf{L}_0^{1/2}\right)_{sm}\boldsymbol{\beta}_m(\mathbf{F}\mathbf{L}_0^{1/2})_{jn}\boldsymbol{\beta}_n]. \tag{14}$$

We recall the useful identities: if $M_p = \int_{-\infty}^{\infty} \eta^p \exp(-\eta^2)d\eta$, then $M_0 = \sqrt{\pi}$, $M_2 = M_0/2$, and $M_4 = 3M_0/4$. Then

$$\left(\frac{\delta \mathcal{F}_{\text{el}}}{\delta \mathbf{x}}\right)_i = -\left(\frac{1}{2}\rho_c k T\right)\frac{\partial (\mathbf{L}^{-1}\mathbf{F}\mathbf{L}_0)_{ip}}{\partial \boldsymbol{\alpha}_p} \tag{15}$$

or

$$\frac{\delta \mathcal{F}_{\text{el}}}{\delta \mathbf{x}} = -\left(\frac{1}{2}\rho_c k T\right)\nabla_{\boldsymbol{\alpha}} \cdot (\mathbf{L}^{-1}\mathbf{F}\mathbf{L}_0). \tag{16}$$

Proceeding similarly,

$$\frac{\delta \mathcal{F}_{\text{el}}}{\delta S} = \pi^{-3/2}\left(\frac{1}{2}\rho_c k T\right)\int d^3\boldsymbol{\beta} \exp(-\boldsymbol{\beta} \cdot \boldsymbol{\beta})\frac{1}{(1 - \mu S)^2}\left[\boldsymbol{\beta}^T \mathbf{L}_0^{1/2}\mathbf{F}^T\mathbf{F}\mathbf{L}_0^{1/2}\boldsymbol{\beta} - \frac{3(1 + 2\mu^2 S^2)}{(1 + 2\mu S)^2}(\boldsymbol{\beta}^T \mathbf{L}_0^{1/2}\mathbf{F}^T \mathbf{n})^2\right]$$

$$+ \pi^{-3/2} \left(\frac{1}{2} \rho_c kT \right) \int d^3\boldsymbol{\beta} \exp(-\boldsymbol{\beta} \cdot \boldsymbol{\beta}) \frac{-3\mu^2 S}{(1 - \mu S)(1 + 2\mu S)}$$

$$= \left(\frac{1}{2} \rho_c kT \right) \frac{1}{2(1 - \mu S)^2} \left[\mathrm{tr}(\mathbf{FL}_0 \mathbf{F}^T) - \frac{3(1 + 2\mu^2 S^2)}{(1 + 2\mu S)^2} \mathrm{tr}(\mathbf{nn}^T \mathbf{FL}_0 \mathbf{F}^T) \right] - \left(\frac{1}{2} \rho_c kT \right) \frac{3\mu^2 S}{(1 - \mu S)(1 + 2\mu S)}, \quad (17)$$

and

$$\frac{\delta \mathcal{F}_{\mathrm{el}}}{\delta \mathbf{n}} = \left(\frac{1}{2} \rho_c kT \right) \pi^{-3/2} \int d^3\boldsymbol{\beta} \exp(-\boldsymbol{\beta} \cdot \boldsymbol{\beta}) \frac{-6\mu S}{(1 - \mu S)(2\mu S + 1)} \left[(\mathbf{n}^T \mathbf{FL}_0^{1/2} \boldsymbol{\beta}) \mathbf{FL}_0^{1/2} \boldsymbol{\beta} - (\mathbf{n}^T \mathbf{FL}_0^{1/2} \boldsymbol{\beta})^2 \mathbf{n} \right]. \quad (18)$$

For simplicity, we denote $\mathbf{G} = \mathbf{FL}_0^{1/2}$. The pth element of $\int d^3\boldsymbol{\beta} \exp(-|\boldsymbol{\beta}|^2)(\mathbf{n}^T \mathbf{G}\boldsymbol{\beta})\mathbf{G}\boldsymbol{\beta}$ is $\frac{\pi^{3/2}}{2} \mathbf{n}_i \mathbf{G}_{ij} \mathbf{G}_{pk} \delta_{jk} = \frac{\pi^{3/2}}{2} \mathbf{G}_{pk} \mathbf{G}_{ki}^T \mathbf{n}_i$. Therefore,

$$\int d^3\boldsymbol{\beta} \exp(-\boldsymbol{\beta} \cdot \boldsymbol{\beta})(\mathbf{n}^T \mathbf{G}\boldsymbol{\beta})\mathbf{G}\boldsymbol{\beta} = \frac{\pi^{3/2}}{2} \mathbf{GG}^T \mathbf{n}$$

$$= \frac{\pi^{3/2}}{2} \mathbf{FL}_0 \mathbf{F}^T \mathbf{n}.$$

Moreover, as $(\mathbf{n}^T \mathbf{FL}_0^{1/2} \boldsymbol{\beta})^2 = \boldsymbol{\beta}^T \mathbf{L}_0^{1/2} \mathbf{F}^T \mathbf{nn}^T \mathbf{FL}_0^{1/2} \boldsymbol{\beta}$, one gets

$$\int d^3\boldsymbol{\beta} \exp(-\boldsymbol{\beta} \cdot \boldsymbol{\beta})(\mathbf{n}^T \mathbf{FL}_0^{1/2} \boldsymbol{\beta})^2 = \frac{\pi^{3/2}}{2} \mathrm{tr}(\mathbf{nn}^T \mathbf{FL}_0 \mathbf{F}^T).$$

Consequently,

$$\frac{\delta \mathcal{F}_{\mathrm{el}}}{\delta \mathbf{n}} = \left(\frac{1}{2} \rho_c kT \right) \frac{-3\mu S}{(1 - \mu S)(1 + 2\mu S)}$$
$$\times [\mathbf{FL}_0 \mathbf{F}^T - \mathrm{tr}(\mathbf{nn}^T \mathbf{FL}_0 F^T)\mathbf{I}]\mathbf{n}.$$

2. Derivatives of nematic free energy density

The nematic free energy can be approximated by

$$F_{\mathrm{nem}} = \int d^3\boldsymbol{\alpha} \left(\frac{1}{2} C_a S^2 - \frac{1}{3} C_b S^3 + \frac{1}{4} C_c S^4 \right).$$

The derivative of the free energy density with respect to S is

$$\frac{\delta \mathcal{F}_{\mathrm{nem}}}{\delta S} = C_a S - C_b S^2 + C_c S^3,$$

and the derivatives with respect to $\mathbf{x}$ and $\mathbf{n}$ are all zero.

3. Derivatives of volume preserving term in the free energy

The volume conserving term does not depend on $\dot{\mathbf{x}}$, S, $\mathbf{n}$, $\dot{S}$, and $\dot{\mathbf{n}}$. We want to find $\delta \mathcal{F}_{\mathrm{vol}}/\delta \mathbf{x}$. Proceeding as before, we obtain

$$\lim_{\epsilon \to 0} \frac{1}{\epsilon} (F_{\mathrm{vol}}[\mathbf{x} + \epsilon \mathbf{y}] - F_{\mathrm{vol}}[\mathbf{x}])$$
$$= \Lambda \int d^3\boldsymbol{\alpha} \left[\mathrm{tr} \left(\mathbf{F}^{-1} \frac{\partial \mathbf{y}}{\partial \boldsymbol{\alpha}} \right) (J - 1)J \right], \quad (19)$$

and, after integrating by parts and requiring $J = 1$ on the boundary, we obtain

$$\frac{\delta \mathcal{F}_{\mathrm{vol}}}{\delta \mathbf{x}} = -\boldsymbol{\nabla}_{\boldsymbol{\alpha}} \cdot (\Lambda (J - 1)J \mathbf{F}^{-T}). \quad (20)$$

4. Derivatives of Rayleigh dissipation

We write the dissipation as

$$\mathcal{R} = \int d^3\boldsymbol{\alpha} \left(\frac{1}{2} \gamma_1 \mathbf{D} : \mathbf{D} + \gamma_2 \mathbf{D} : \dot{\mathbf{Q}} + \frac{1}{2} \gamma_3 \dot{\mathbf{Q}} : \dot{\mathbf{Q}} \right)$$
$$= \int d^3\boldsymbol{\alpha} (\mathcal{R}_{d1} + \mathcal{R}_{d2} + \mathcal{R}_{d3}). \quad (21)$$

Since $\mathcal{R}_1$ is independent of $\mathbf{x}$, S, $\mathbf{n}$, $\dot{S}$, and $\dot{\mathbf{n}}$, we calculate the derivative $\delta \mathcal{R}_{d1}/\delta \dot{\mathbf{x}}$. Proceeding as before, we obtain

$$\frac{d}{d\epsilon} [\mathcal{R}_1(\dot{\mathbf{x}} + \epsilon \dot{\mathbf{y}})]_{\epsilon=0} = \gamma_1 \int d^3\boldsymbol{\alpha} [\mathrm{tr}(\mathbf{DF}^{-T} \boldsymbol{\nabla}_{\boldsymbol{\alpha}} \dot{\mathbf{y}}^T)], \quad (22)$$

and integration by parts gives

$$\frac{\delta \mathcal{R}_{d1}}{\delta \dot{\mathbf{x}}} = -\gamma_1 \boldsymbol{\nabla}_{\boldsymbol{\alpha}} \cdot (\mathbf{DF}^{-T}).$$

A calculation similar to that above shows that

$$\frac{\delta \mathcal{R}_{d2}}{\delta \dot{\mathbf{x}}} = -\gamma_2 \boldsymbol{\nabla}_{\boldsymbol{\alpha}} \cdot (\dot{\mathbf{Q}} \mathbf{F}^{-T}).$$

We note that $\dot{\mathbf{Q}} = \dot{S}(\frac{3}{2} \mathbf{nn}^T - \frac{1}{2} \mathbf{I}) + \frac{3}{2} S(\dot{\mathbf{n}} \mathbf{n}^T + \mathbf{n}\dot{\mathbf{n}}^T)$. Then simple calculations yield

$$\frac{\delta \mathcal{R}_{d2}}{\delta \dot{S}} = \gamma_2 \mathbf{D} : \left(\frac{3}{2} \mathbf{nn}^T - \frac{1}{2} \mathbf{I} \right)$$

and

$$\frac{\delta \mathcal{R}_{d2}}{\delta \dot{\mathbf{n}}} = 3\gamma_2 S[\mathbf{Dn} - (\mathbf{n}^T \mathbf{Dn})\mathbf{n}].$$

Similarly, we obtain

$$\frac{\delta \mathcal{R}_{d3}}{\delta \dot{S}} = \frac{3}{2} \gamma_3 \dot{S},$$

and

$$\frac{\delta \mathcal{R}_{d3}}{\delta \dot{\mathbf{n}}} = \frac{9}{2} \gamma_3 S^2 \dot{\mathbf{n}}.$$

By combining these, we obtain the derivatives of the Rayleigh dissipation as

$$\frac{\delta \mathcal{R}_d}{\delta \dot{\mathbf{x}}} = -\gamma_1 \boldsymbol{\nabla}_{\boldsymbol{\alpha}} \cdot (\mathbf{DF}^{-T}) - \gamma_2 \boldsymbol{\nabla}_{\boldsymbol{\alpha}} \cdot (\dot{\mathbf{Q}} \mathbf{F}^{-T}),$$

$$\frac{\delta \mathcal{R}_d}{\delta \dot{S}} = \gamma_2 \mathbf{D} : \left(\frac{3}{2} \mathbf{nn}^T - \frac{1}{2} \mathbf{I} \right) + \frac{3}{2} \gamma_3 \dot{S},$$

and

$$\frac{\delta \mathcal{R}_d}{\delta \dot{\mathbf{n}}} = 3\gamma_2 S[\mathbf{Dn} - (\mathbf{n}^T \mathbf{Dn})\mathbf{n}] + \frac{9}{2} \gamma_3 S^2 \dot{\mathbf{n}}.$$

5. *The equations of motion*

We now derive the equations of motion governing the time evolution of the velocity $\mathbf{u}$ of the elastomer and of the nematic order parameter $\mathbf{Q}$, expressed in terms of S and $\mathbf{n}$. Recall that the dynamics is given by

$$\frac{\partial}{\partial t}\frac{\delta \mathcal{E}_{\text{kin}}}{\delta \dot{\mathbf{x}}} + \frac{\delta \mathcal{F}}{\delta \mathbf{x}} + \frac{\delta \mathcal{R}_d}{\delta \dot{\mathbf{x}}} = 0, \tag{23}$$

$$\frac{\delta \mathcal{F}}{\delta S} + \frac{\delta \mathcal{R}_d}{\delta \dot{S}} = 0, \tag{24}$$

and

$$\frac{\delta \mathcal{F}}{\delta \mathbf{n}} + \frac{\delta \mathcal{R}_d}{\delta \dot{\mathbf{n}}} = 0, \tag{25}$$

where $\mathcal{E}_{\text{kin}}$ is the kinetic energy density, $\mathcal{F}$ is the free energy density, and $\mathcal{R}_d$ is the Rayleigh dissipation function.

First consider the Lagrangian flow map $\mathbf{x}(\boldsymbol{\alpha},t)$. Recasting the kinetic energy from the current to the initial configuration gives

$$\begin{aligned}
E_{\text{kin}} &= \int_{\Omega(t)} d^3\mathbf{x}\, \mathcal{E}_{\text{kin}} \\
&= \int_{\Omega(t)} d^3\mathbf{x} \left(\frac{1}{2}\rho_m(\mathbf{x},t)\mathbf{u}(\mathbf{x},t)\cdot\mathbf{u}(\mathbf{x},t)\right) \\
&= \int_{\Omega(0)} d^3\boldsymbol{\alpha} \left(\frac{1}{2}\rho_m(\mathbf{x}(\boldsymbol{\alpha},t),t)\dot{\mathbf{x}}(\boldsymbol{\alpha},t)\cdot\dot{\mathbf{x}}(\boldsymbol{\alpha},t)J(\boldsymbol{\alpha},t)\right) \\
&= \int_{\Omega(0)} d^3\boldsymbol{\alpha} \left(\frac{1}{2}\rho_m(\boldsymbol{\alpha},0)\dot{\mathbf{x}}(\boldsymbol{\alpha},t)\cdot\dot{\mathbf{x}}(\boldsymbol{\alpha},t)\right), \tag{26}
\end{aligned}$$

where we use mass conservation $\rho_m(\mathbf{x}(\boldsymbol{\alpha},t),t)J(\boldsymbol{\alpha},t) = \rho_m(\boldsymbol{\alpha},0)$, with ρ_m the mass density of the liquid crystal elastomer. We then have

$$\frac{\delta \mathcal{E}_{\text{kin}}}{\delta \dot{\mathbf{x}}} = \rho_m \dot{\mathbf{x}} = \rho_m \mathbf{u}, \tag{27}$$

and subsequently

$$\frac{\partial}{\partial t}(\rho_m \mathbf{u}) + \frac{\delta(\mathcal{F}_{\text{el}} + \mathcal{F}_{\text{nem}} + \mathcal{F}_{\text{vol}})}{\delta \mathbf{x}} + \frac{\delta \mathcal{R}_d}{\delta \dot{\mathbf{x}}} = 0,$$

or

$$\begin{aligned}
\rho_m \frac{\partial \mathbf{u}}{\partial t} &= \left(\frac{1}{2}\rho_c kT\right)\boldsymbol{\nabla}_{\boldsymbol{\alpha}}\cdot(\mathbf{L}^{-1}\mathbf{F}\mathbf{L}_0) + \boldsymbol{\nabla}_{\boldsymbol{\alpha}}\cdot(\Lambda(J-1)J\mathbf{F}^{-T}) \\
&\quad + \gamma_1\boldsymbol{\nabla}_{\boldsymbol{\alpha}}\cdot(\mathbf{D}\mathbf{F}^{-T}) + \gamma_2\boldsymbol{\nabla}_{\boldsymbol{\alpha}}\cdot(\dot{\mathbf{Q}}\mathbf{F}^{-T}). \tag{28}
\end{aligned}$$

We remark that the coupling of strain and orientational order, the salient aspect of liquid crystal elastomers, is implicit in the first term of the right-hand side. Since $\mathbf{L} = \mathbf{I} + 2\mu\mathbf{Q}$, spatial variations of the order parameter give rise to stresses, and in turn, to elastomer motion.

Next, consider the dynamics of the order parameter expressed through the variables S and $\mathbf{n}$. Since the Lagrangian $\mathcal{L}$ does not depend on $\dot{S}$ or $\dot{\mathbf{n}}$, the equations of motion give

$$\frac{\delta(\mathcal{F}_{\text{el}} + \mathcal{F}_{\text{nem}} + \mathcal{F}_{\text{vol}})}{\delta S} + \frac{\delta \mathcal{R}_d}{\delta \dot{S}} = 0,$$

$$\frac{\delta(F_{\text{el}} + F_{\text{nem}} + F_{\text{vol}})}{\delta \mathbf{n}} + \frac{\delta \mathcal{R}_d}{\delta \dot{\mathbf{n}}} = 0,$$

or

$$\begin{aligned}
\frac{3\gamma_3}{2}\frac{\partial S}{\partial t} &= -\left(\frac{1}{2}\rho_c kT\right)\frac{1}{2(1-\mu S)^2} \\
&\quad \times\left[\operatorname{tr}(\mathbf{F}\mathbf{L}_0\mathbf{F}^T) - \frac{3(2\mu^2 S^2 + 1)}{(2\mu S + 1)^2}\operatorname{tr}(\mathbf{n}\mathbf{n}^T\mathbf{F}\mathbf{L}_0\mathbf{F}^T)\right] \\
&\quad + \left(\frac{1}{2}\rho_c kT\right)\frac{3\mu^2 S}{(1-\mu S)(1+2\mu S)} \\
&\quad - \left[C_a S - C_b S^2 + C_c S^3\right] - \gamma_2\mathbf{D}:\left(\frac{3}{2}\mathbf{n}\mathbf{n}^T - \frac{1}{2}\mathbf{I}\right), \tag{29}
\end{aligned}$$

and

$$\begin{aligned}
\frac{9\gamma_3 S^2}{2}\frac{\partial \mathbf{n}}{\partial t} &= \left(\frac{1}{2}\rho_c kT\right)\frac{3\mu S}{(1-\mu S)(1+2\mu S)} \\
&\quad \times(\mathbf{F}\mathbf{L}_0\mathbf{F}^T - \operatorname{tr}(\mathbf{n}\mathbf{n}^T\mathbf{F}\mathbf{L}_0\mathbf{F}^T)\mathbf{I})\mathbf{n}. \tag{30}
\end{aligned}$$

Equations (28), (29), and (30) are the equations of motion for the nematic liquid crystal elastomer system.

We make these equations of motion nondimensional by introducing the following dimensionless quantities:

$$\mathbf{u}' = \frac{\mathbf{u}}{u}, \qquad \boldsymbol{\alpha}' = \frac{\boldsymbol{\alpha}}{b}, \qquad t' = \frac{t}{\tau},$$

where b is the step length of liquid crystal and constants u and τ are to be determined.

Equation (28) becomes

$$\begin{aligned}
\rho_m\frac{u}{\tau}\frac{\partial \mathbf{u}'}{\partial t'} &= \left(\frac{1}{2}\rho_c kT\right)\frac{1}{b}\boldsymbol{\nabla}_{\boldsymbol{\alpha}'}\cdot(\mathbf{L}^{-1}\mathbf{F}\mathbf{L}_0) \\
&\quad + \frac{1}{b}\boldsymbol{\nabla}_{\boldsymbol{\alpha}'}\cdot(\Lambda(J-1)J\mathbf{F}^{-T}) \\
&\quad + \gamma_1\frac{u}{b^2}\boldsymbol{\nabla}_{\boldsymbol{\alpha}'}\cdot((\boldsymbol{\nabla}_{\boldsymbol{\alpha}'}\mathbf{u}\mathbf{F}^{-1} + \mathbf{F}^{-T}\boldsymbol{\nabla}_{\boldsymbol{\alpha}'}\mathbf{u}^T)\mathbf{F}^{-T}), \tag{31}
\end{aligned}$$

where we let $\gamma_2 = 0$ for simplicity for the time being. Letting $u = b/\tau$ and $\tau = \gamma_3/\rho_c kT$, the above equation reads:

$$\begin{aligned}
\lambda\frac{\partial \mathbf{u}'}{\partial t'} &= \frac{1}{2}\boldsymbol{\nabla}_{\boldsymbol{\alpha}'}\cdot(\mathbf{L}^{-1}\mathbf{F}\mathbf{L}_0) + \boldsymbol{\nabla}_{\boldsymbol{\alpha}'}\cdot(\Lambda'(J-1)J\mathbf{F}^{-T}) \\
&\quad + \frac{\gamma_1}{2\gamma_3}\boldsymbol{\nabla}_{\boldsymbol{\alpha}'}\cdot((\boldsymbol{\nabla}_{\boldsymbol{\alpha}'}\mathbf{u}\mathbf{F}^{-1} + \mathbf{F}^{-T}\boldsymbol{\nabla}_{\boldsymbol{\alpha}'}\mathbf{u}^T)\mathbf{F}^{-T}), \tag{32}
\end{aligned}$$

where $\lambda = \rho_c kT\rho_m b^2/\gamma_3^2$ and $\Lambda' = \Lambda/\rho_c kT$.

With this choice of parameters we have

$$\begin{aligned}
\frac{\partial S}{\partial t'} &= -\frac{1}{6(1-\mu S)^2}\left[\operatorname{tr}(\mathbf{F}\mathbf{L}_0\mathbf{F}^T)\right. \\
&\quad \left. - \frac{3(1+2\mu^2 S^2)}{(1+2\mu S)^2}\operatorname{tr}(\mathbf{n}\mathbf{n}^T\mathbf{F}\mathbf{L}_0\mathbf{F}^T)\right] \\
&\quad + \frac{\mu^2 S}{(1-\mu S)(1+2\mu S)} \\
&\quad + \frac{200}{3}\left[-5\left(\frac{\text{Tem}}{360}-1\right)S + 4S^2 - 5S^3\right], \tag{33}
\end{aligned}$$

where $\mathrm{Tem} = \mathrm{Tem}(\boldsymbol{\alpha}', t')$ is a temperature function depending on location $\boldsymbol{\alpha}'$ and time t'.

$$\frac{\partial \mathbf{n}}{\partial t'} = \frac{\mu S}{3S^2(1 - \mu S)(1 + 2\mu S)}[\mathbf{FL_0F}^T - \mathrm{tr}(\mathbf{nn}^T\mathbf{FL_0F}^T)\mathbf{I}]\mathbf{n}. \tag{34}$$

This equation preserves the length of the director $\mathbf{n}$, as required.

Finally, the deformation matrix $\mathbf{F}$ satisfies

$$\frac{\partial \mathbf{F}}{\partial t'} = \nabla_{\boldsymbol{\alpha}'}\mathbf{u}, \tag{35}$$

while (again) the Lagrangian map $\mathbf{x}$ satisfies

$$\frac{\partial \mathbf{x}}{\partial t'} = \mathbf{u}. \tag{36}$$

III. NUMERICAL RESULTS

We present simulations of the dynamics of an LCE sample—using Eqs. (32)–(36) when exposed to external illumination and subject to two different boundary conditions. The LCE sample is taken as box shaped, as in Fig. 1(a). In the first set of simulations, zero-stress boundary conditions are imposed over the sample surface (i.e., the sample is "free"). In the second case, one end of the sample is anchored to a wall, with the remainder free. In either case, gravitational loads are neglected. Numerically, the difference between these two cases lies only in the treatment of the velocity on one face of the sample. However, the dynamics the two cases present are quite different, as observed in [4].

A. Methods

To discretize the equations of motion, one needs to consider suitable schemes for approximating both spatial derivatives and time derivatives. Here we employ the spectral Chebyshev polynomial method to discretize spatial derivatives with high efficiency and accuracy [14]. As for time discretization, we use a popular implicit-explicit scheme that is a combination of the second-order Adams-Bashforth scheme for the explicit term and the Crank-Nicolson scheme for the implicit term [14–16].

We now outline the Chebyshev polynomial method and the implicit-explicit time-stepping method. The dynamics is simulated in the Lagrangian domain $\Omega(0) = [-a,a] \times [-b,b] \times [-c,c]$, which by definition is fixed in time. This is trivially mapped to the cube $[-1,1]^3$. This cubic domain is then discretized in each direction on the Gauss-Lobatto points (e.g., in the first coordinate, $\boldsymbol{\alpha}_{1,j} = \cos(j\pi/N), j = 0(1)N$). This allows allows spatially dependent fields, such as $\mathbf{u}$ or $\mathbf{F}$, that are represented discretely on these points to also be represented efficiently, via Fast Fourier Transform (FFT), as finite sums of Chebychev polynomials [14]. The Chebychev representation can then be used to provide highly accurate derivative approximations upon the grid. To illustrate in one dimension, let $u(x)$ be defined on $[-1,1]$ and approximated by $u_N(x) = \sum_{p=0}^{N} a_p T_p(x)$ where T_p is the pth Chebychev polynomial. The a_p's are determined by requiring u_N to interpolate u at the Gauss-Lobatto points. This Chebychev
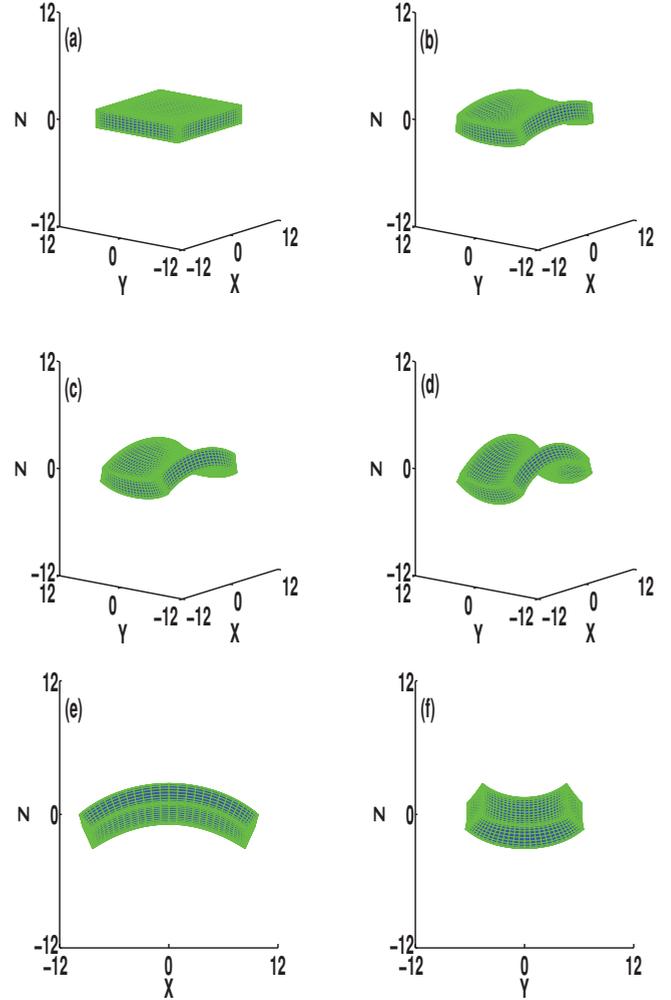
FIG. 1. (Color online) The shape evolution of the LCE sample due to an inhomogeneous distribution of temperature. Panel (a) shows the initial state of the LCE sample, panels (b) and (c) are two intermediate states, and panel (d) represents the equilibrium state. Panels (e) and (f) present the shapes of the LCE sample at the equilibrium state [panel (d)] from two different perspectives. In this experiment, the temperature drops linearly from the top of the LCE sample to its bottom and is distributed uniformly on each horizontal slice. The temperature spatial distribution is maintained during the evolution process. This numerical experiment simulates the physical one shown in Fig. 4 in [4].

representation allows us to construct approximations to $u^{(p)}(x)$, at the Gauss-Lobatto points, that have the form

$$u_N^{(p)}(x_i) = \sum_{j=0}^{N} d_{ij}^{(p)} u_N(x_j), \quad i = 0(1)N,$$

where $[d_{ij}^{(p)}]$ is the the pth Chebyshev differentiation matrix (see [14]). Since our three-dimensional grid is of tensor product form, derivatives are easily gotten by application of such matrices along lines of constant coordinate of the discretized data.

The LCE dynamics in which we are interested takes place in the overdamped regime; that is, the Reynolds number, $\lambda\gamma_3/\gamma_1$, associated with viscous fluid damping is very small. Hence,
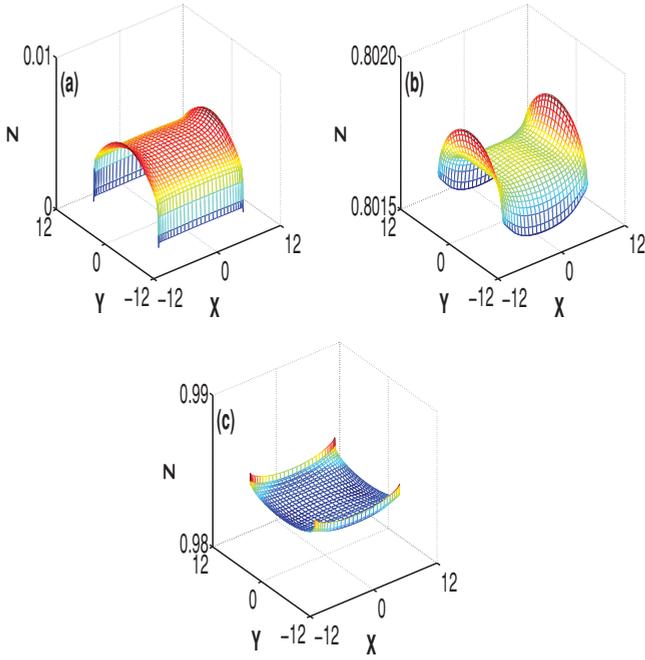
FIG. 2. (Color online) The order parameter (S) distribution for the top [panel (a)], middle [panel (b)], and bottom [panel (c)] horizontal slices of the LCE sample at the equilibrium state. The order parameter is close to zero on the top slice while it is close to one on the bottom slice. It is the inhomogeneous distribution of the order parameter that leads to internal stress and thus results in the shape changes of the LCE sample. Moreover, the order parameter slightly varies on each of these slices, suggesting the elastic effect on the order parameter.

FIG. 3. (Color online) The nematic direction (**n**) distribution for the top slice of the LCE sample at the initial and the equilibrium states. Panel (a) represents the nematic direction on the top slice at the initial state. Panels (b), (c), and (d) illustrate the nematic direction on the top slice for different perspectives at the equilibrium state.

if we retain $\mathbf{u}_t$ in the dynamics, we must implicitly treat the viscous damping so as to avoid extreme constraints on the time step that would be imposed by using an explicit scheme. Here, we choose a popular implicit-explicit method which is described for a typical time-dependent equation:

$$\frac{du}{dt} = f(u) + vg(u),$$

with $f(\cdot)$, $g(\cdot)$ being the nonlinear and linear terms, respectively. We apply a second-order Adams-Bashforth method to the nonlinear terms and Crank-Nicholson averaging to the linear term, or

$$\frac{u^{n+1} - u^n}{\Delta t} = \frac{3}{2} f(u^n) - \frac{1}{2} f(u^{n-1}) + \frac{v}{2} [g(u^{n+1}) + g(u^n)],$$

(37)

where Δt is the time-step size and u^n is the approximation of $u(n\Delta t)$. This scheme involves solution values on three time levels. The first time step is taken by setting $u^{-1} = u^0 = u(0)$ (see [14]).

B. Treatment of interior and boundary points

Note that Eqs. (33) and (34) involve no spatial derivatives and are solved directly by the second-order Adams-Bashforth method without using the Chebyshev approximation. More care must be taken with the momentum Equation (32) as it is a source of stiffness in the numerical treatment and its advancement involves boundary conditions. This is an
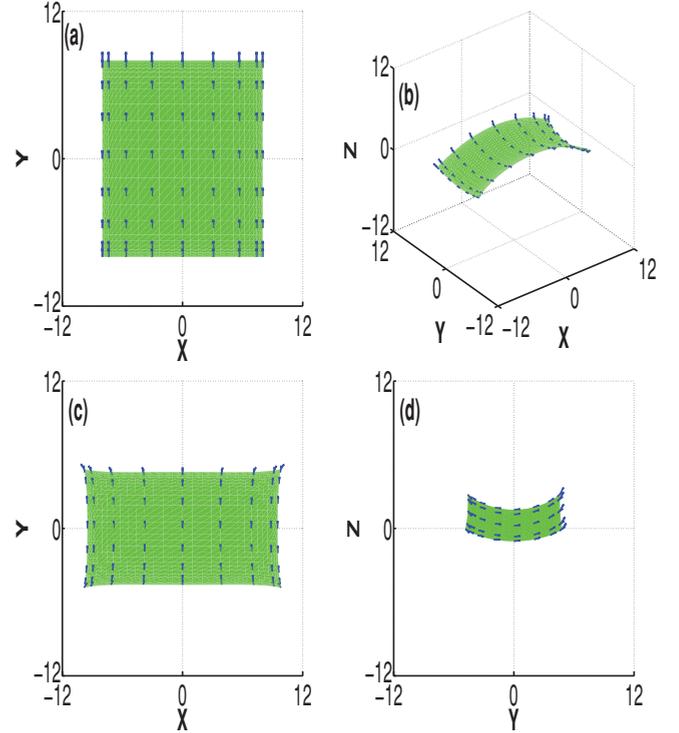
important issue, since distinct boundary conditions result in completely different behaviors of the LCE sample. In what follows, we mainly discuss how to handle the equation for both boundary and interior points.

The three-dimensional grid using the Gauss-Labatto points is composed of both surface and interior points. To update the velocity at the interior points, we need to solve a large linear system gotten by applying the implicit-explicit method for the velocity Equation (32), coupling this to boundary conditions. For a "free" LCE sample, this is a condition of zero stress, which under discretization of velocity gradients in the viscous stress provides a coupling condition of the boundary velocities to the interior velocities.

The velocity Equation (32) can be discretized as follows:

$$\frac{\mathbf{u}^{n+1} - \mathbf{u}^n}{\Delta t} = \frac{3}{2} \left[\frac{1}{\lambda} \nabla \cdot \left(\Lambda(J-1)J\mathbf{F}^{-T} + \frac{1}{2}\mathbf{L}^{-1}\mathbf{F}\mathbf{L}_0 \right) \right]^n$$
$$- \frac{1}{2} \left[\frac{1}{\lambda} \nabla \cdot \left(\Lambda(J-1)J\mathbf{F}^{-T} + \frac{1}{2}\mathbf{L}^{-1}\mathbf{F}\mathbf{L}_0 \right) \right]^{n-1}$$
$$+ \frac{\gamma_1}{4\gamma_3} \nabla \cdot [(\nabla\mathbf{u}\mathbf{F}^{-1} + \mathbf{F}^{-T}\nabla\mathbf{u}^T)\mathbf{F}^{-T}]^{n+1}$$
$$+ \frac{\gamma_1}{4\gamma_3} \nabla \cdot [(\nabla\mathbf{u}\mathbf{F}^{-1} + \mathbf{F}^{-T}\nabla\mathbf{u}^T)(\mathbf{F}^{-T})]^n,$$

where $[\cdot]^n$ represents the value at $n\Delta t$. This equation amounts to a large linear system for the unknown velocity $\mathbf{u}^{n+1}$ at the interior points. Couplings within the matrix arise through expansion of spatial derivatives (that is, gradients and a tensor

divergence) through the Chebyshev expansion of the velocity. Despite the many entries in the matrix generated through the derivatives, the matrix is nonetheless rather sparse, and we explicitly construct the entries and store this sparse matrix. Once the boundary conditions are appropriately integrated, we solve this large system using the iterative Generalized minimal residual (GMRES) method [21].

Surface values of velocity are either additional unknowns or are specified as in the case of having an anchored surface where $\mathbf{u} = 0$ on that face. The former is the case of the zero-stress boundary condition. In the Lagrangian frame, using Nanson's formula [18], this boundary condition can be written as

$$\left[\Lambda(J-1)\mathbf{I} + \frac{1}{2}\mathbf{L}^{-1}\mathbf{F}\mathbf{L}_0\mathbf{F}^T \right] \cdot J\mathbf{F}^{-T}\nu_0$$
$$+ \frac{\gamma_1}{2\gamma_3}[(\boldsymbol{\nabla}_{\boldsymbol{\alpha}}\mathbf{u}\mathbf{F}^{-1} + \mathbf{F}^{-T}\boldsymbol{\nabla}_{\boldsymbol{\alpha}}\mathbf{u}^T)] \cdot J\mathbf{F}^{-T}\nu_0 = \mathbf{0}, \quad (38)$$

where ν_0 denotes the outward normal unit vector to the time invariant surface $\partial\Omega(0) = \partial\Omega$. In our method, this vector ν_0 takes different values at the side, edge, and corner points on the boundary of the cubic volume of the LCE sample. Specifically, ν_0 takes value from the set

$$\{(\pm 1,0,0),(0,\pm 1,0),(0,0,\pm 1)\}$$

at the side points,

$$\left\{ \frac{1}{\sqrt{2}}(\pm 1,\pm 1,0), \frac{1}{\sqrt{2}}(\pm 1,\mp 1,0), \frac{1}{\sqrt{2}}(\pm 1,0,\pm 1), \right.$$
$$\left. \frac{1}{\sqrt{2}}(\pm 1,0,\mp 1), \frac{1}{\sqrt{2}}(0,\pm 1,\pm 1), \frac{1}{\sqrt{2}}(0,\pm 1,\mp 1) \right\}$$

at the edge points, and

$$\left\{ \frac{1}{\sqrt{3}}(\pm 1,\pm 1,\pm 1), \frac{1}{\sqrt{3}}(\pm 1,\pm 1,\mp 1), \right.$$
$$\left. \frac{1}{\sqrt{3}}(\mp 1,\pm 1,\pm 1), \frac{1}{\sqrt{3}}(\mp 1,\pm 1,\mp 1) \right\}$$

at the corner points.

We rewrite the boundary condition Equation (38) as

$$\left[(\boldsymbol{\nabla}_{\boldsymbol{\alpha}}\mathbf{u}\mathbf{F}^{-1} + \mathbf{F}^{-T}\boldsymbol{\nabla}_{\boldsymbol{\alpha}}\mathbf{u}^T) \right]\mathbf{F}^{-T}\nu_0 = \mathbf{A}\nu_0,$$

where $\mathbf{A} = -\frac{2\gamma_3}{\gamma_1}[\frac{1}{2}\mathbf{L}^{-1}\mathbf{F}\mathbf{L}_0 + \Lambda(J-1)J\mathbf{F}^{-T}]$. This boundary condition is evaluated at the $(n+1)$st time step. Given that all of the dynamics equations, bar that for the velocity $\mathbf{u}$, are treated explicitly, we can consider $\mathbf{F}$ and $\mathbf{A}$ as being considered known and the velocity gradients as unknowns. Gradients are either tangential to the sample surface and hence only couple together boundary points (upon approximation of gradients using the Chebyshev representation), or normal to the surface and hence couple together boundary and interior points.

This yields a closed set of equations for $\mathbf{u}^{n+1}$ at the interior points and on those surface upon which a zero-stress boundary condition is imposed. As said above, this system is solved via the GMRES iterative method [21].

C. Simulations

Before proceeding, we discuss the choice of dimensionless parameters. These include the coefficient of acceleration $\lambda = \rho_c kT\rho_m b^2/\gamma_3^2$, the viscosity ratio γ_1/γ_3, the coefficient for
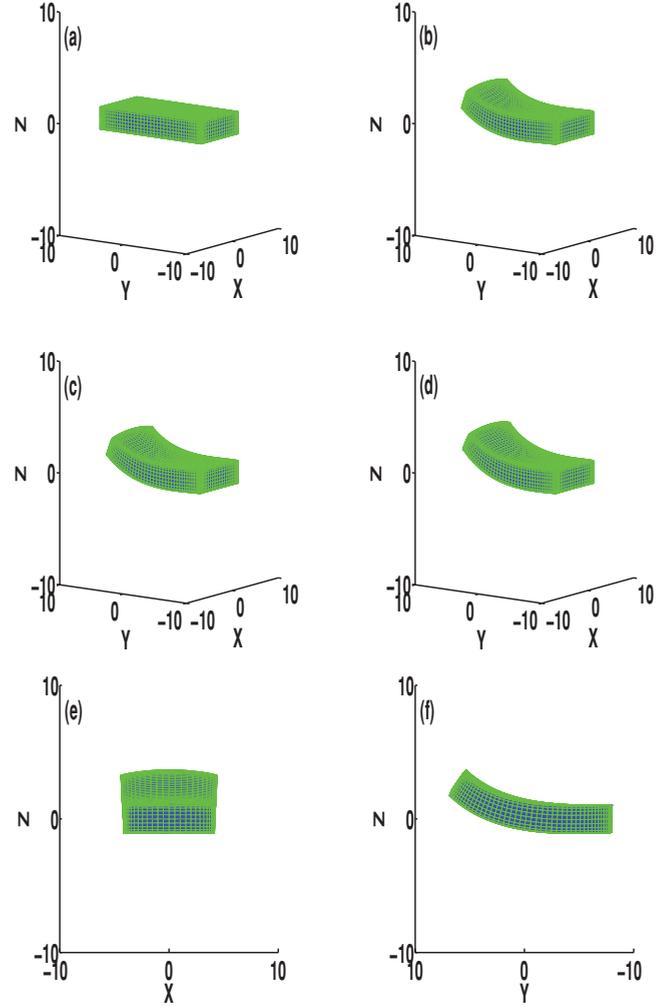
FIG. 4. (Color online) The shape evolution of the LCE sample due to an inhomogeneous distribution in temperature. Panel (a) shows the initial state of the LCE sample, panels (b) and (c) are two intermediate states, and panel (d) represents the equilibrium state. Panels (e) and (f) present the shapes of the LCE sample at the equilibrium state [panel (d)] from two different perspectives. This experiment shares the same condition as the previous simulation in Fig. 1 except that a lateral surface of the LCE sample is fixed. This numerical experiment simulates the physical one shown in Fig. 2 in [4].

volume conservation Λ, and the anisotropy of step length μ appearing in the tensor $\mathbf{L}$. Taking typical values [4], we have $\lambda = O(10^{-3})$ and $\gamma_1/\gamma_3 = O(10^{1-2})$. Hence, inertial forces in the material are quite small. Ideally, we should choose a very large value of Λ to enforce material incompressibility, but this imposes a severe time-step restriction in our numerical scheme. We use $\Lambda = 10^3$. The parameter μ lies in the range $[0,1.0]$. A large value of μ corresponds to a large order parameter, which accelerates the deformation process of the LCE sample. We use $\mu = 0.9$ in the simulations.

We now consider the simulated dynamics of the first case of a "free" LCE sample being exposed to illumination from above. In this simulation, the sample size is $8 \times 8 \times 1$, with $N_1 = 32$, $N_2 = 32$, and $N_3 = 10$ points being used in each direction, respectively. The initial data used were $\mathbf{u}_0 \equiv \mathbf{0}$,
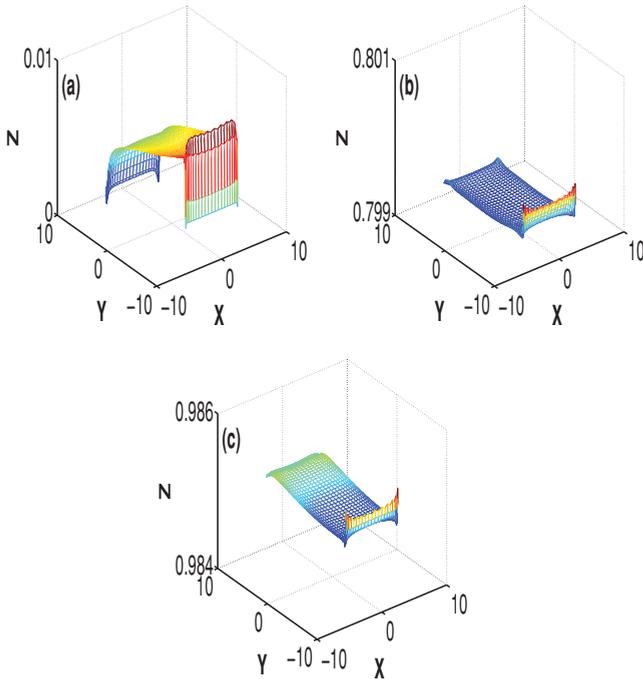
FIG. 5. (Color online) The order parameter (S) distribution for the top [panel (a)], middle [panel (b)], and bottom [panel (c)] horizontal slices of the LCE sample at the equilibrium state. The order parameter is close to zero on the top slice while it is close to one on the bottom slice. It is the nonhomogeneous distribution of the order parameter that leads to internal stress and thus results in the shape changes of the LCE sample. Moreover, the order parameter slightly varies on each of these slices and oscillates near the fixed lateral surface of the LCE sample, suggesting both the elastic effect and the effect due to the anchored surface on the order parameter.

FIG. 6. (Color online) The nematic direction (**n**) distribution for the top slice of the LCE sample at the initial and the equilibrium states. Panel (a) represents the nematic direction on the top slice at the initial state. Panels (b), (c), and (d) illustrate the nematic direction on the top slice for different perspectives at the equilibrium state.

$\mathbf{n}_0 \equiv \hat{\mathbf{y}}$, $\mathbf{X}_0 \equiv \boldsymbol{\alpha}$, and $s_0 \equiv \bar{s}$, where $\bar{s}$ is the constant value found as the minimizer of the Landau–de Gennes free energy density (3) given a uniform temperature throughout the sample corresponding to 290 K (in dimensional units). As discussed earlier, we neglect thermal diffusion and assume that the temperature is uniform in each horizontal slice of the sample, decreasing linearly from top (420 K) to bottom (290 K). Although this is an approximation, we find that the dynamics driven by this temperature field captures the salient aspects of the observed response [4].

Figure 1 shows the deformation process from this initial configuration. The final result—a saddle shape—is very similar to that observed in the experiment of Palffy-Muhoray *et al.* (see Fig. 4 of [4]). The evolution proceeds in three stages: an initially slow and small bending, followed by rapid and large deformation, and finally a slow relaxation to a terminal shape. This dynamics is driven by the evolution of the orientational order parameter, s, as it adjusts its values (low on the top and higher on the bottom) in response to the imposed temperature gradient. The inhomogeneous spatial distribution of orientational order, especially through the thickness of the LCE sample, gives rise to large stresses and hence creates a strong driving force toward changing the shape of the sample.

The last two plots of Fig. 1 show the late-time-deformed sample from two different perspectives. Here one finds that
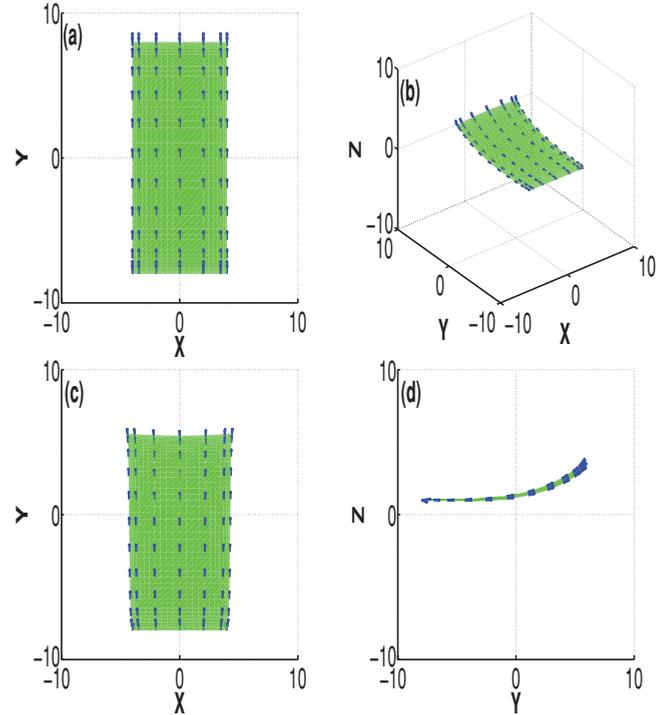
the length along the y axis has become shorter, while that along the x axis has increased. This is again due to the time evolution of the order parameter. At the top surface, given its increased temperature, the degree of order of the rodlike mesogens decreases. Since these mesogens are initially aligned along the y direction, this loss of order leads to a contraction of the sample along the y direction and corresponding extensions along the x and z directions. Since the temperature is different on each horizontal layer, the degree of contraction also is also different. It is this difference in contraction and expansion through the thickness of LCE sample that results in the observed saddle-shaped deformation.

The simulation shows that as the dynamics progresses, the order parameter in each horizontal layer converges to nearly constant values essentially determined by the temperature assigned to that layer [see Eq. (33)], though somewhat affected also by elastic effects induced by coupling to **n**. This is illustrated in Fig. 2, which shows that the order parameter generally assumes smaller values at the top and larger values on the bottom, but also varies (slightly) within each layer.

We also study the dynamics of nematic director **n**. In Fig. 3, the nematic director on the top surface of the sample is compared at the initial and equilibrium states. For the equilibrium state, three perspectives are given from which one can easily discern the evolution of the nematic director. Similar director distributions on the other layers of the sample can be observed.

The dynamics of the second simulation can be explored similarly. In this simulation, all initial conditions and spatial

temperature distributions are as in the first example, except that one lateral surface of the sample is fixed, and the dimensions of the LCE sample are now $4 \times 8 \times 1$, which is narrower in the x direction. In this simulation, we used $N_1 = 24$, $N_2 = 48$, and $N_3 = 10$ in x,y,z directions, respectively.

Figure 4 shows the deformation process. Again, the result is very similar to that observed in actual experiment (see Fig. 2 of [4]) with the sample bending upward at its free end. As the in first simulation, the deformation proceeds through three stages, with the sample also contracting along the initial nematic direction and extending in the other two orthogonal directions. This is illustrated the Figs. 4(e) and 4(f). All these phenomena share the underlying physics as in the first simulation.

In Fig. 5, the order parameter distributions within the top, middle, and bottom layers of the sample in the equilibrium state are shown. The order parameter within each layer is nearly constant within each layer, though with small oscillations caused by boundary effects. However, when compared with Fig. 2 for the first simulation, one finds that the basic deformation pattern is different and asymmetric due to the anchoring boundary condition used in this experiment.

Figure 6, shows the disposition of the nematic director on the top surface of the LCE sample, again comparing the initial and the equilibrium states. For the equilibrium state, three perspectives are shown. We see that the nematic director bends upward, and the bending increases with distance from the fixed side of the sample. Similar director dynamics are observed in the other layers.

IV. CONCLUSIONS

In this paper, we derived the equations of motion for an LCE sample in the long-wave limit and implemented their numerical solution. Our numerical experiments demonstrate that the model is capable of describing the dynamics of nematic LCEs when exposed to external stimuli such as illumination.

[1] P. G. de Gennes, C. R. Acad. Sci., Ser. B **281**, 101 (1975).

[2] H. Finkelmann, H. Kock, and G. Rehage, Makromol. Chem. Rapid Commun. **2**, 317 (1981).

[3] H. R. Brand and H. Pleiner, Physica A **208**, 359 (1994).

[4] P. Palffy-Muhoray, M. Camacho-Lopez, H. Finkelmann, and M. Shelley, Nat. Mater. **3**, 307 (2004).

[5] M. Warner and E. M. Teretjev, *Liquid Crystal Elastomers* (Clarendon Press, Oxford, 2003).

[6] Y. Yu, M. Nakano, and T. Ikeda, Nature (London) **425**, 145 (2003).

[7] J. Cviklinski, A. R. Tajbakhsh, and E. M. Terentjev, Eur. Phys. J. E **9**, 427 (2002).

[8] S. M. Clarke, A. R. Tajbakhsh, E. M. Terentjev, and M. Warner, Phys. Rev. Lett. **86**, 4044 (2001).

[9] H. Finkelmann, E. Nishikawa, G. G. Pereira, and M. Warner, Phys. Rev. Lett. **87**, 015501 (2001).

[10] P. Palffy-Muhoray, W. Cao, M. Moreira, B. Taheri, and A. Munoz, Phil. Trans. R. Soc. A **364**, 2747 (2006).

[11] E. M. Terentjev, A. Hotta, S. M. Clarke, and M. Warner, Phil. Trans. R. Soc. A **361**, 653 (2003).

[12] T. J. White, J. J. Koval, V. P. Tondiglia, L. V. Natarajan, R. A. Vaia, S. Serak, V. Grozhik, N. Tabirian, and T. J. Bunning, Proc. SPIE **6654**, 665403 (2007).

[13] R. Ennis, L. C. Malacarne, P. Palffy-Muhoray, and M. Shelley, Phys. Rev. E **74**, 061802 (2006).

[14] R. Peyret, *Spectral Methods for Incompressible Viscous Flow* (Springer-Verlag, New York, 2002).

[15] U. R. Acher, S. J. Ruuth, and B. T. R. Wetton, SIAM J. Numer. Anal. **32**, 797 (1995).

[16] B. Gustafsson, H. O. Kreiss, and J. Oliger, *Time Dependent Problems and Difference Methods* (John Wiley and Sons, New York, 1995).

[17] P. G. de Gennes and J. Prost, *The Physics of Liquid Crystals* (Oxford University Press, Oxford, 1993).

[18] G. Holzapfel, *Nonlinear Solid Mechanics* (Wiley, Chichester, 2000).

[19] A. N. Beris and B. J. Edwards, *The Thermodynamics of Flowing Systems* (Oxford University Press, Oxford, 1994), p. 95.

[20] C. Oldano and G. Barbero, Phys. Lett. A **110**, 213 (1985).

[21] Y. Saad and M. H. Schultz, SIAM J. Sci. Stat. Comput. **7**, 856 (1986).